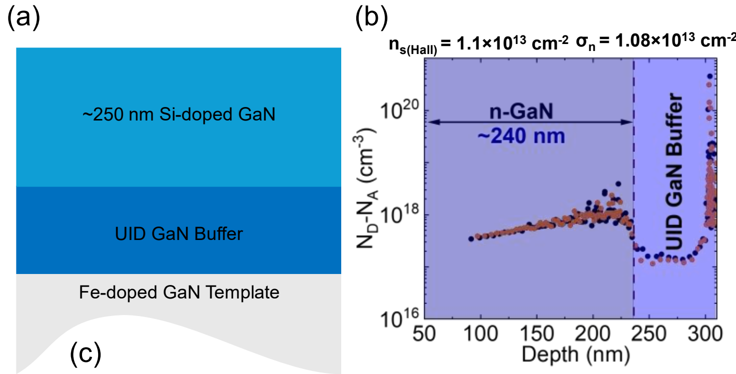

(c)

	Hall Mobility (cm²/V•s)	Sheet Charge (cm⁻²)	Sheet Resistance (Ω/□)	Resistivity (Ω•cm)
Device 1	419	1.1×10^13	1.35×10^3	67.71×10^-3
Device 2	454	1.1×10^13	1.25×10^3	62.26×10^-3
Device 3	462	1.1×10^13	1.2×10^3	60.2×10^-3
Device 4	420	1.1×10^13	1.35×10^3	67.56×10^-3

FIG.1. (a) n-GaN epilayer grown by NH_3-MBE. (b) Doping vs. depth profile via MOS C-V. (c) Electrical properties of n-GaN from room temperature Hall effect measurements.

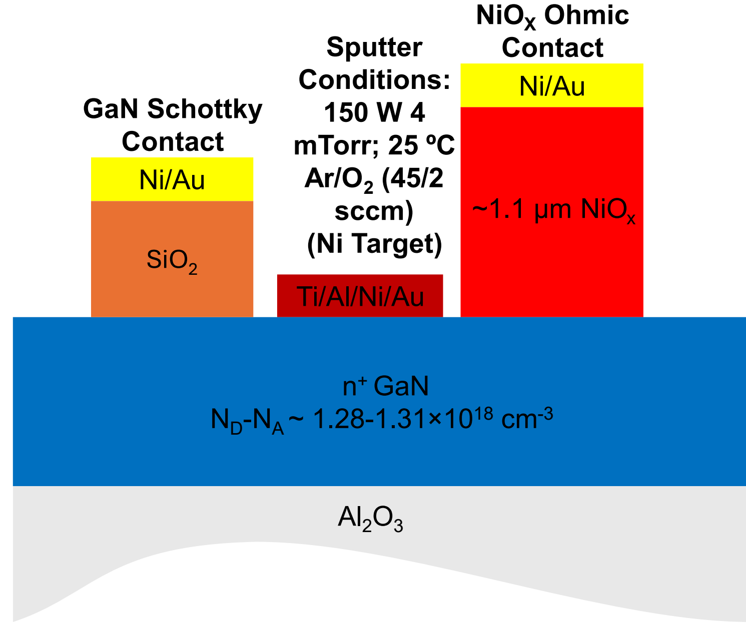

FIG.2. MOS C-V and sputtered NiO_x diode on n^+ GaN-on-sapphire template used for acceptor (N_a) concentration extraction

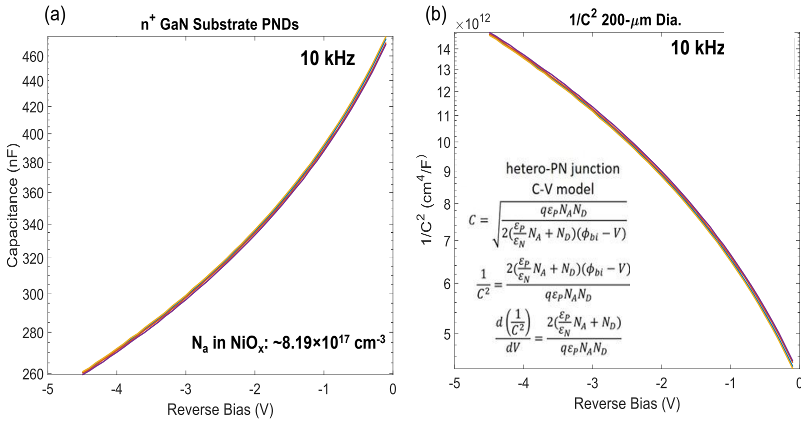

FIG.3. (a) C-V characteristics of NiO_x/n^+ GaN heterojunction diode at 10 kHz on 200-µm dia. devices (b). $1/C^2$ vs. reverse bias of the heterojunction diode at 10 kHz on 200-µm dia. devices.

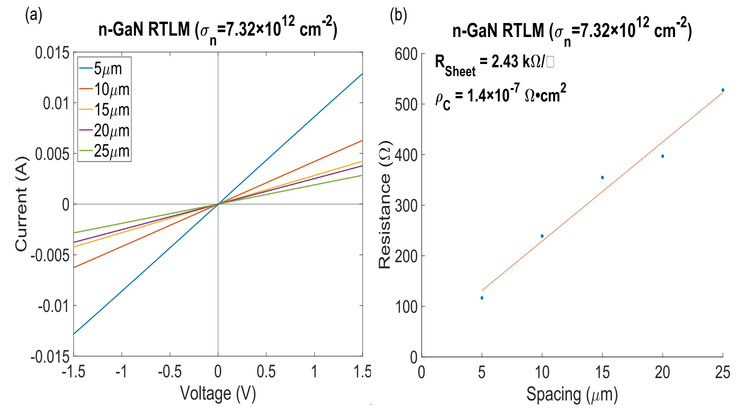

FIG.4. (a) I-V characteristics of etched n-GaN Ohmic contact from circular transmission line measurements (CTLM) (b). Resistance fits from CTLM with R_{sheet} and ρ_c extracted.

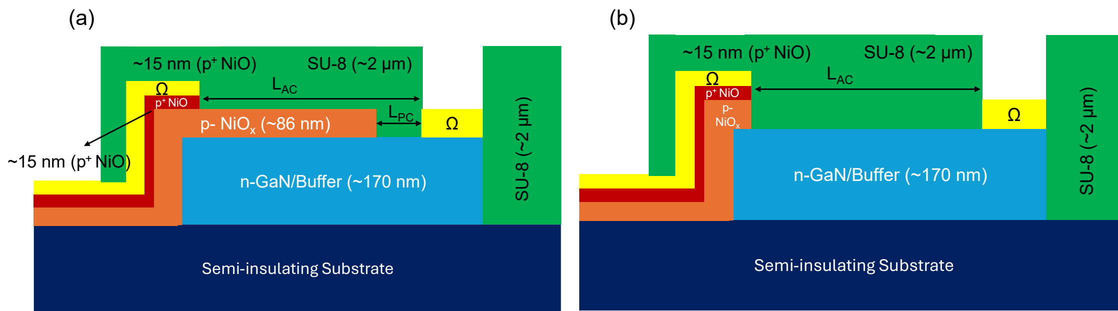

FIG.5. (a) NiO_x/GaN super-heterojunction. (b) NiO_x/GaN super-heterojunction reference structure without NiO_x extension.

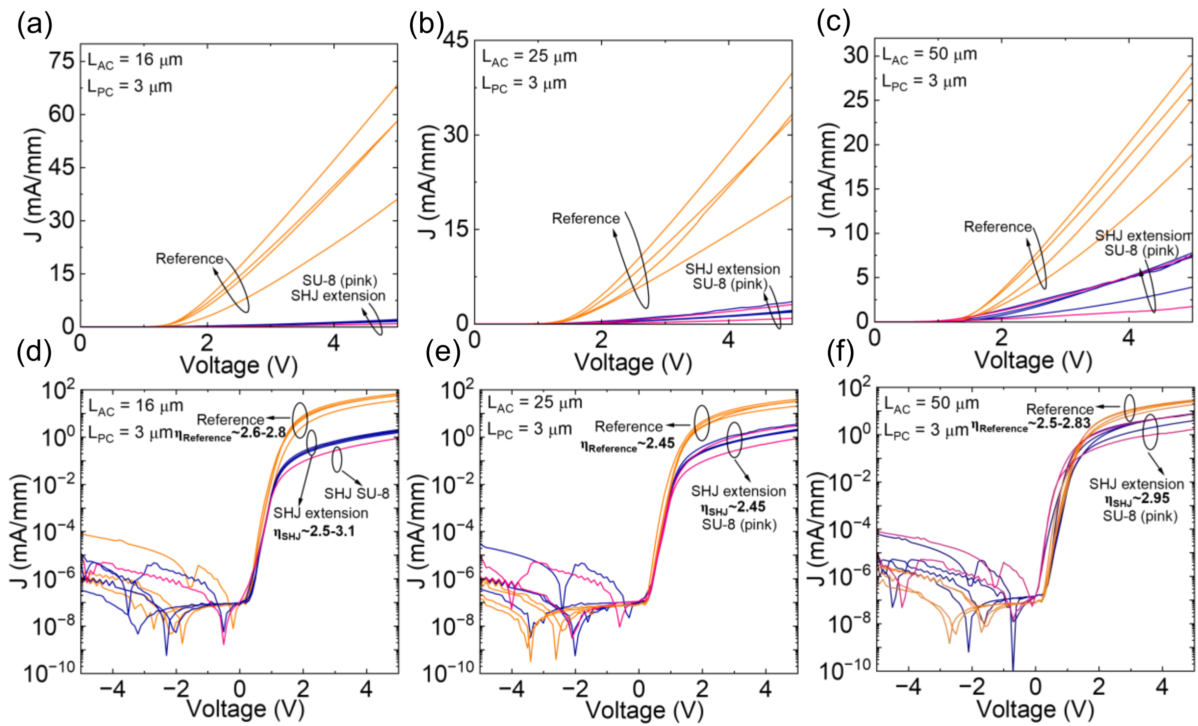

FIG.6. (a-c) Linear forward J-V characteristics of NiO_x/GaN SHJ with anode-to-cathode distance of 16, 25, and 50-μm. (d-f) Semilog J-V forward characteristics of NiO_x/GaN SHJ with anode-to-cathode distance of 16, 25, and 50-μm with ideality factor extracted.

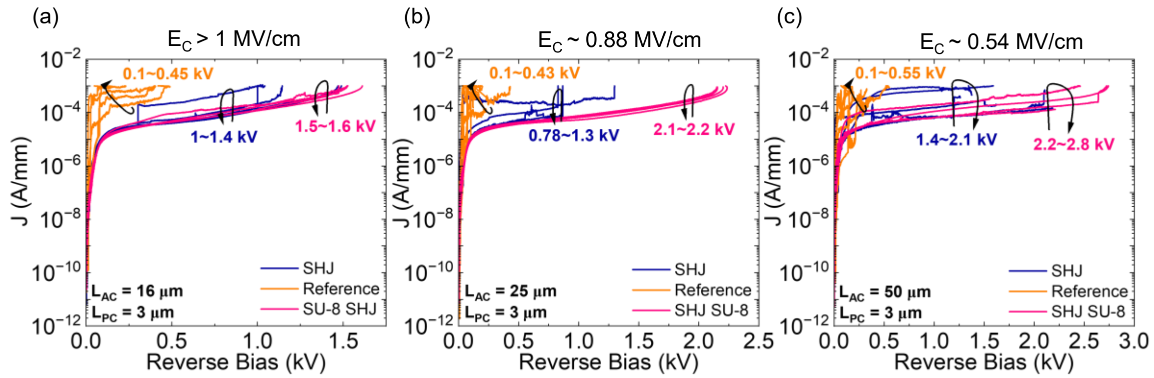

FIG.7. Breakdown characteristics of NiO_x/GaN SHJ, reference structure, and SHJ passivated by SU-8 with anode-to-cathode distance of (a) 16, (b) 25, and (c) 50-μm.

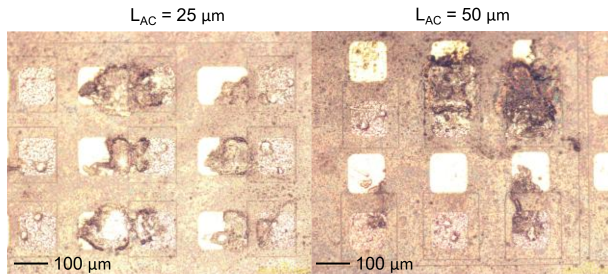

FIG.8. Optical microscopic images of NiO_x/GaN SHJ submerged in silicone oil after catastrophic breakdown under reverse bias.

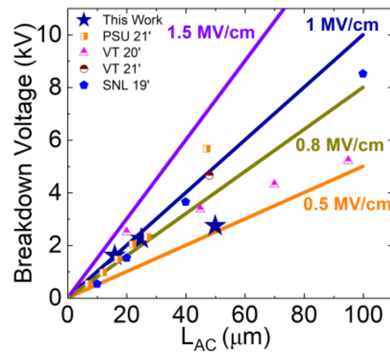

FIG.9. Benchmarking of NiO_x/GaN SHJ with existing GaN-based lateral superjunction devices.